

POTENTIAL SINGULARITY OF THE AXISYMMETRIC EULER EQUATIONS WITH C^α INITIAL VORTICITY FOR A LARGE RANGE OF α . PART II: THE N -DIMENSIONAL CASE

THOMAS Y. HOU* AND SHUMAO ZHANG†

Abstract. In Part II of this sequence to our previous paper for the 3-dimensional Euler equations [8], we investigate potential singularity of the n -dimensional axisymmetric Euler equations with C^α initial vorticity for a large range of α . We use the adaptive mesh method to solve the n -dimensional axisymmetric Euler equations and use the scaling analysis and dynamic rescaling method to examine the potential blow-up and capture its self-similar profile. Our study shows that the n -dimensional axisymmetric Euler equations with our initial data develop finite-time blow-up when the Hölder exponent $\alpha < \alpha^*$, and this upper bound α^* can asymptotically approach $1 - \frac{2}{n}$. Moreover, we introduce a stretching parameter δ along the z -direction. Based on a few assumptions inspired by our numerical experiments, we obtain $\alpha^* = 1 - \frac{2}{n}$ by studying the limiting case of $\delta \rightarrow 0$. For the general case, we propose a relatively simple one-dimensional model and numerically verify its approximation to the n -dimensional Euler equations. This one-dimensional model sheds useful light to our understanding of the blowup mechanism for the n -dimensional Euler equations. As shown in [8], the scaling behavior and regularity properties of our initial data are quite different from those of the initial data considered by Elgindi in [6].

Key words. n -dimensional axisymmetric Euler equations, finite-time blow-up

AMS subject classifications. 35Q31, 76B03, 65M60, 65M06, 65M20

1. Introduction. The question regarding the global regularity of the 3D incompressible Euler equations with smooth initial data has been widely recognized as a major open problem in partial differential equations (PDEs). Despite a lot of previous efforts, this question remains unresolved until very recently when Chen and Hou [2] provided a rigorous justification of the Luo-Hou blow-up scenario with smooth initial data and boundary [14, 15]. In 2021, Elgindi [6] showed that the 3D axisymmetric Euler equations with no swirl can develop finite-time singularity for a class of C^α initial vorticity with very small $\alpha > 0$. Inspired by Elgindi's work, we provided numerical evidence for a potential finite-time self-similar singularity of the 3D axisymmetric Euler equations with no swirl and with C^α initial vorticity for a large range of $\alpha \in (0, 1/3)$ in [8] using a different class of initial data.

In this paper, we extend the numerical study in [8] of the potential finite-time singularity in axisymmetric Euler equations with no swirl from the 3-dimensional case to the higher dimensional case. We will also provide more interesting observations that shed useful light on the potential blowup mechanism. As in our previous paper [8], we will use an adaptive mesh method and the dynamic rescaling formulation [7, 1, 3] to study the self-similarity and scaling properties of the potential singularity. By introducing a parameter δ to control the stretching of the computational domain and the initial data in the z -axis, we find that the n -dimensional axisymmetric Euler equations with C^α initial vorticity can develop potential finite-time blow-up when α is smaller than some critical value α^* , and this critical value α^* can asymptotically approach $1 - \frac{2}{n}$ as $\delta \rightarrow 0$. This result supports Conjecture 8 of [5] and generalizes it to the high-dimensional case.

More specifically, we denote by ω^θ as the angular vorticity and ψ^θ as the angular

*Department of Computing and Mathematical Sciences, California Institute of Technology, Pasadena, CA (hou@cms.caltech.edu).

†Department of Computing and Mathematical Sciences, California Institute of Technology, Pasadena, CA (shumaoz@caltech.edu).

stream function. We will use the same change of variables as in [8]:

$$\omega^\theta(r, z) = r^\alpha \omega_1(r, z), \quad \psi^\theta(r, z) = r \psi_1(r, z).$$

We make the following self-similar blowup ansatz for ω_1 and ψ_1 :

$$\begin{aligned} \omega_1(x, t) &\approx \frac{1}{(T-t)^{c_\omega}} \Omega \left(\frac{x-x_0}{(T-t)^{c_l}} \right), \\ \psi_1(x, t) &\approx \frac{1}{(T-t)^{c_\psi}} \Psi \left(\frac{x-x_0}{(T-t)^{c_l}} \right), \end{aligned}$$

for some constants c_ω , c_ψ , c_l , x_0 and T . Here T is the blow-up time, and x_0 is the location of the self-similar blow-up. The parameters c_ω , c_ψ , c_l are called scaling factors. Based on our numerical observations, we make a few assumptions about the potential blow-up, and study the limiting case of $\delta \rightarrow 0$. Using a formal asymptotic analysis inspired by our numerical results, we derive the following scaling relationships for c_l and c_ω as $\delta \rightarrow 0$:

$$c_l = \frac{n-1}{n-2-n\alpha}, \quad c_\omega = \frac{n-2-\alpha}{n-2-n\alpha}.$$

In the limiting case of $\delta \rightarrow 0$, we obtain $\alpha^* = 1 - \frac{2}{n}$, which agrees with our numerical results. Moreover, we propose a relatively simple one-dimensional model that focuses on the behavior of the n -dimensional axisymmetric Euler equations along the z -axis. Our numerical experiments confirm that the one-dimensional model is a good approximation of the original n -dimensional Euler equations, and can develop approximately the same potential finite-time blow-up as the original Euler equations. This one-dimensional model can be used as a simplified model to study the finite-time blow-up of the n -dimensional Euler equations rigorously.

There have been many previous studies of potential finite time singularity of the 3D incompressible Euler equations with smooth initial data. These include both analytic studies and numerical investigations. We refer to Part I of this sequence [8] for more detailed discussions.

The rest of the paper is organized as follows. In Section 2, we describe the setup of the problem and our numerical method. In Section 3, we present convincing numerical evidences for a potential self-similar blowup. In Section 4, we study the relationship between the Hölder exponent α and the space dimension n in the potential self-similar blowup. We investigate the possible mechanism leading to the potential finite time blowup of the n -dimensional Euler equations in Section 5. Section 6 is devoted to a one-dimensional model to study the potential self-similar blowup of the n -dimensional axisymmetric Euler equations. Some concluding remarks are drawn in Section 7.

2. Problem set up and numerical method. In this section, we first establish the high-dimensional axisymmetric Euler equations with no swirl, and some basic properties of the equations, then present the initial data, and the boundary conditions that we use in our study.

2.1. High-dimensional axisymmetric Euler equations with no swirl. To start with, we introduce the n -dimensional axisymmetric Euler equations. Let

$$u(x, t) : \mathbb{R}^n \times [0, T) \rightarrow \mathbb{R}^n, \quad \text{and} \quad p(x, t) : \mathbb{R}^n \times [0, T) \rightarrow \mathbb{R},$$

be an n -D vector field of the velocity and an n -D scalar field of the pressure respectively, where $x = (x_1, x_2, \dots, x_n) \in \mathbb{R}^n$. Then the n -dimensional Euler equations can be written as

$$(2.1a) \quad u_t + u \cdot \nabla u = -\nabla p,$$

$$(2.1b) \quad \nabla \cdot u = 0.$$

Next, we consider a hyper-cylindrical coordinate system $(r, \theta_1, \dots, \theta_{n-2}, z)$, which is related to the Cartesian coordinate system (x_1, x_2, \dots, x_n) via the following relation

$$\begin{aligned} x_1 &= r \cos \theta_1, \\ x_2 &= r \sin \theta_1 \cos \theta_2, \\ &\vdots \\ x_{n-1} &= r \sin \theta_1 \cdots \sin \theta_{n-2} \\ x_n &= z. \end{aligned}$$

The hyper-cylindrical coordinate system is simply the direct product of a $(n-1)$ -D spherical coordinate system with a 1D Cartesian coordinate system. The frame of the hyper-cylindrical coordinate system can be expressed in the Cartesian coordinate as

$$\begin{aligned} e_r &= (\cos \theta_1, \sin \theta_1 \cos \theta_2, \dots, \sin \theta_1 \cdots \cos \theta_{n-2}, \sin \theta_1 \cdots \sin \theta_{n-2}, 0), \\ e_{\theta_1} &= (-\sin \theta_1, \cos \theta_1 \cos \theta_2, \dots, \cos \theta_1 \cdots \cos \theta_{n-2}, \cos \theta_1 \cdots \sin \theta_{n-2}, 0), \\ &\vdots \\ e_{\theta_{n-2}} &= (0, 0, \dots, -\sin \theta_{n-2}, \cos \theta_{n-2}, 0), \\ e_z &= (0, 0, \dots, 0, 0, 1). \end{aligned}$$

Similar to the 3D case, we call an n -D vector field v to be axisymmetric if the following ansatz applies

$$v = v^r(r, z)e_r + v^{\theta_1}(r, z)e_{\theta_1} + v^z(r, z)e_z.$$

In other words, v^r , v^{θ_1} , and v^z are only functions of (r, z) . For such vector field, the calculus on the curvilinear coordinate [4] of $(r, \theta_1, \dots, \theta_{n-2}, z)$ gives

$$\begin{aligned} \nabla \cdot v &= v_r^r + \frac{n-2}{r}v^r + \frac{(n-3)\cot \theta_1}{r}v^{\theta_1} + v_z^z, \\ (v \cdot \nabla)v &= \left(v^r v_r^r + v^z v_z^r - \frac{1}{r}v^{\theta_1} v^{\theta_1} \right) e_r + \left(v^r v_r^{\theta_1} + v^z v_z^{\theta_1} + \frac{1}{r}v^r v^{\theta_1} \right) e_{\theta_1} \\ &\quad + (v^r v_r^z + v^z v_z^z) e_z. \end{aligned}$$

We can see that if there is non-zero ‘‘swirl’’ u^{θ_1} in the initial condition for dimension $n \neq 3$, then the incompressibility condition $\nabla \cdot u = 0$ will inevitably introduce the dependence on θ_1 for the equations, which implies that we cannot obtain a truly axisymmetric Euler equations for dimension greater than 3. Note that when $n = 3$, the incompressibility condition does not introduce any trouble since the third term in $\nabla \cdot v$ vanishes exactly for $n = 3$ even if there is swirl.

Therefore, to derive the n -dimensional axisymmetric Euler equations with $n > 3$, we need to impose the ‘‘no swirl’’ assumption $u^{\theta_1} = 0$. Luckily, the ‘‘no swirl’’

assumption will be preserved dynamically by the n -D axisymmetric Euler equations. We remark that the axisymmetric Euler equations offer tremendous computational saving, which enables us to investigate potential finite time singularity for the general n -dimensional Euler equations using our current computational resources.

Thus, the axisymmetric n -D Euler equations with no swirl can be written in the vorticity-stream function form as

$$(2.2a) \quad \omega_t^\theta + u^r \omega_r^\theta + u^z \omega_z^\theta = \frac{n-2}{r} u^r \omega^\theta,$$

$$(2.2b) \quad -\psi_{rr}^\theta - \psi_{zz}^\theta - \frac{n-2}{r} \psi_r^\theta + \frac{n-2}{r^2} \psi^\theta = \omega^\theta,$$

$$(2.2c) \quad u^r = -\psi_z^\theta, \quad u^z = \frac{n-2}{r} \psi^\theta + \psi_r^\theta,$$

where we introduce the angular vorticity ω^θ and angular stream function ψ^θ as $\omega^\theta = u_z^r - u_r^z$ and $-\Delta \psi^\theta = \omega^\theta$, similar to the 3D axisymmetric Euler equations.

Since we plan to use C^α continuous initial data for the angular vorticity ω^θ , we follow the same change-of-variables as in [8]:

$$(2.3) \quad \omega^\theta(r, z) = r^\alpha \omega_1(r, z), \quad \psi^\theta(r, z) = r \psi_1(r, z).$$

Using (ω_1, ψ_1) , an equivalent form of the n -D axisymmetric Euler equations with no swirl is given below

$$(2.4a) \quad \omega_{1,t} + u^r \omega_{1,r} + u^z \omega_{1,z} = -(n-2-\alpha) \psi_{1,z} \omega_1,$$

$$(2.4b) \quad -\psi_{1,rr} - \psi_{1,zz} - \frac{n}{r} \psi_{1,r} = \omega_1 r^{\alpha-1},$$

$$(2.4c) \quad u^r = -r \psi_{1,z}, \quad u^z = (n-1) \psi_1 + r \psi_{1,r}.$$

Roughly speaking, the dimension n controls the strength of the vortex stretching term $-(n-2-\alpha) \psi_{1,z} \omega$ and the z -advection speed $u^z = (n-1) \psi_1 + r \psi_{1,r}$. It also modifies the Poisson equation for ψ_1 . It seems natural to conjecture that the singularity formation will be more likely in the high-dimensional case because of the stronger vortex stretching term $-(n-2-\alpha) \psi_{1,z} \omega$.

Similar to the 3D case, the n -D axisymmetric Euler equations also admit the conservation of the kinetic energy E , which is defined as

$$E = \frac{1}{2} \int_0^1 \int_0^{1/2} (|u^r|^2 + |u^z|^2) r^{n-2} dr dz.$$

2.2. Self-similar solution. The self-similar blow-up solutions for nonlinear PDEs are of particular interest in our study. A self-similar solution is when the local profile of the solution remains nearly unchanged in time after rescaling the spatial and the temporal variables of the physical solution. For example, for (2.4), the self-similar profile is the ansatz

$$(2.5) \quad \begin{aligned} \omega_1(x, t) &\approx \frac{1}{(T-t)^{c_\omega}} \Omega \left(\frac{x-x_0}{(T-t)^{c_l}} \right), \\ \psi_1(x, t) &\approx \frac{1}{(T-t)^{c_\psi}} \Psi \left(\frac{x-x_0}{(T-t)^{c_l}} \right), \end{aligned}$$

for some constants c_ω , c_ψ , c_l , x_0 and T . Here T is the blow-up time, and x_0 is the location of the self-similar blow-up. The parameters c_ω , c_ψ , c_l are called scaling factors.

Similar to the 3D case, the axisymmetric n -D Euler equations with no swirl (2.4) admits the following scaling invariant property: if (ω_1, ψ_1) is a solution of (2.4), then

$$(2.6) \quad \left\{ \frac{1}{\lambda^{\alpha\tau}} \omega_1 \left(\frac{x}{\lambda}, \frac{t}{\tau} \right), \frac{\lambda}{\tau} \psi_1 \left(\frac{x}{\lambda}, \frac{t}{\tau} \right) \right\}$$

is also a solution.

Thus if we assume the existence of the self-similar solution (2.5), then the new solutions in (2.6) should also admit the same ansatz, regardless of the values of λ and μ . As a result, we must have

$$(2.7) \quad c_\omega = 1 + \alpha c_l, \quad c_\psi = 1 - c_l.$$

Therefore, the self-similar profile (2.6) of (2.4) only has one degree of freedom, for example c_l , in the scaling factors. And as a consequence, we have

$$(2.8) \quad \|\omega^\theta(x, t)\|_{L^\infty} \sim \frac{1}{T-t}, \quad \|\psi_{1,z}(x, t)\|_{L^\infty} \sim \frac{1}{T-t},$$

if the solution is self-similar.

2.3. Boundary conditions, symmetries and initial data. For (2.4), we impose a periodic boundary condition in z with period 1:

$$(2.9) \quad \omega_1(r, z) = \omega_1(r, z + 1), \quad \psi_1(r, z) = \psi_1(r, z + 1).$$

and a pole condition for ψ_1 at $r = 0$ and a no-flow boundary condition for ψ_1 at $r = 1$:

$$(2.10) \quad \psi_{1,r}(0, z) = 0, \quad \psi_1(1, z) = 0.$$

This would allow us to only focus on the cylinder region

$$\mathcal{D}_{\text{cyl}} = \{(r, z) : 0 \leq r \leq 1\}.$$

Here at $r = 0$, $u^r(0, z) = -r\psi_{0,z} = 0$, so there is no need for the boundary condition for ω_1 at $r = 0$. And according to [12, 13], $\psi^\theta = r\psi_1$ is at least C^2 -continuous, so ψ^θ must be an odd function of r , and thus we have the pole condition $\psi_{1,r}(0, z) = 0$. The condition $\psi_1(1, z) = 0$ implies that the no-flow boundary condition $u^r(1, z) = -r\psi_{1,z} = 0$ is satisfied at $r = 1$. Therefore, there is no need to introduce a boundary condition for ω_1 at $r = 1$.

In addition to the boundary conditions, we enforce that (ω_1, ψ_1) are odd functions in z :

$$(2.11) \quad \omega_1(r, z) = -\omega_1(r, -z), \quad \psi_1(r, z) = -\psi_1(r, -z).$$

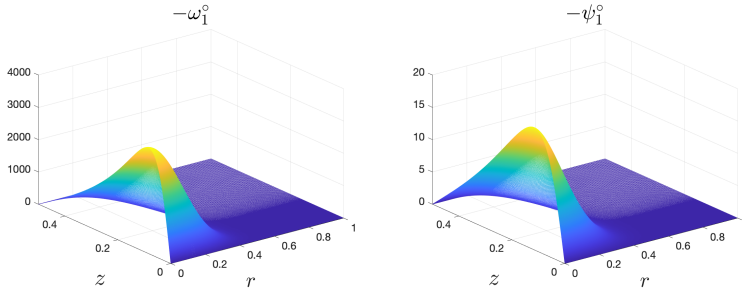
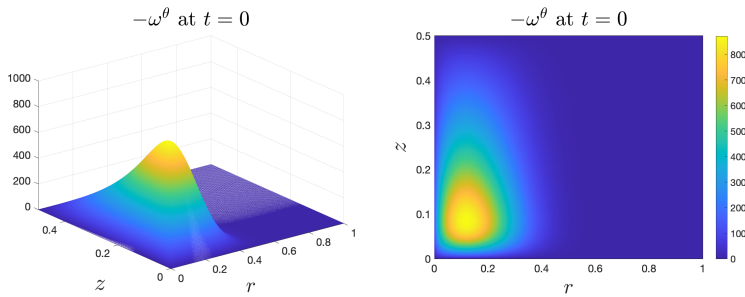
And the n -D Euler equations (2.4) will preserve this symmetry dynamically.

Due to the periodicity and the odd symmetry along the z direction, the equations (2.4) only need to be solved on the half-periodic cylinder

$$\mathcal{D} = \{(r, z) : 0 \leq r \leq 1, 0 \leq z \leq 1/2\}$$

because there is no transport of the flow across its boundaries. Indeed, we have

$$u^r = 0 \quad \text{on} \quad r = 0 \text{ or } 1, \quad \text{and} \quad u^z = 0 \quad \text{on} \quad z = 0 \text{ or } 1/2.$$

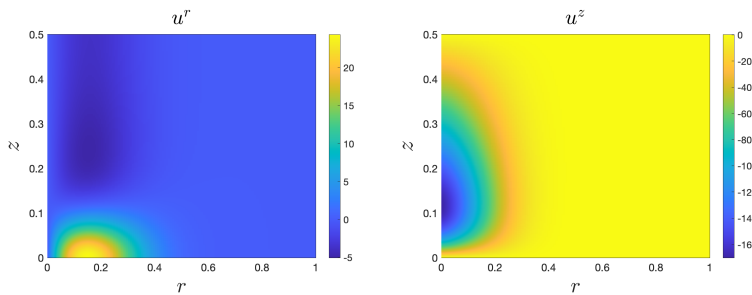
FIG. 1. 3D profiles of the initial value $-\omega_1^\circ$ and $-\psi_1^\circ$.FIG. 2. The initial data for the angular vorticity ω^θ , when $\alpha = 0.5$.

Thus, the boundaries of \mathcal{D} behave like “impermeable walls”.

Following to the choice in [8], we propose the initial data for ω_1 in \mathcal{D} as,

$$(2.12) \quad \omega_1^\circ = \frac{-12000(1-r^2)^{18} \sin(2\pi z)}{1 + 12.5 \sin^2(\pi z)}.$$

Notice that (2.12) has a slightly different denominator compared to the initial data used in [8]. In fact, both choices of the initial data will lead to the similar numerical phenomenon in the 3D or n -D case, as observed in Section 6 of [8]. However, our study shows that it takes less time for (2.12) to develop a potential blow-up, because the initial vorticity will concentrate more near the origin, which helps reduce our computational cost. Thus we use the above initial data in our study. We solve the Poisson equation (2.4b) to get the initial value ψ_1° of ψ_1 .

FIG. 3. Initial velocity fields u^r and u^z .

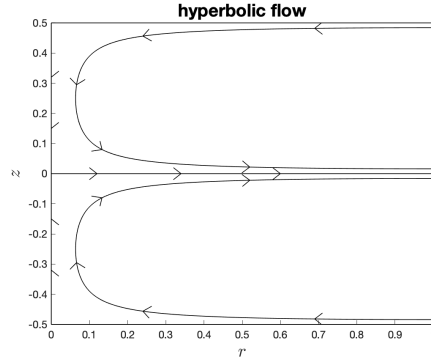


FIG. 4. A heuristic diagram of the hyperbolic flow.

The 3D profiles of $(\omega_1^\circ, \psi_1^\circ)$ can be found in Figure 1. Since most parts of ω_1° and ψ_1° are negative, we negate them for better visual effect when generating figures. In Figure 2, we show the 3D profile and pseudocolor plot of the angular vorticity ω^θ at $t = 0$. We can see that there is a sharp drop to zero of $-\omega^\theta$ near $r = 0$, which is due to the Hölder continuous of ω^θ at $r = 0$.

We plot the initial velocity field u^r and u^z in Figure 3. We can see that u^r is essentially positive near $z = 0$ and negative near $z = 1/2$ when r is small, and u^z is mainly negative when r is small. Such a pattern suggests a hyperbolic flow near $(r, z) = (0, 0)$ as depicted in the heuristic diagram Figure 4, which will extend periodically in z .

Although the initial data are very smooth, the solutions of the n -dimensional Euler equations quickly become very singular and concentrate in a rapidly shrinking region. Therefore, we use the same adaptive mesh method to resolve the singular profile of the solutions as we did in our previous paper [8]. A detailed description of the adaptive mesh method can be found in [7, 16, 19].

In our algorithm, we adopt a second-order implementation for our adaptive mesh method. In Section 3.3 of [8], we present resolution study to confirm the order of accuracy of the adaptive mesh method.

3. Numerical evidence for a potential self-similar singularity. We provide numerical evidence for the finite-time blow-up in the high-dimensional case. We will use the setting $n = 10$, $\alpha = 0.5$ in this section. More exploration of different settings of n and α will be studied in the Section 5 and 6.

3.1. Evidence for a potential singularity. On 1024×1024 spatial resolution, we solve the equations (2.4) until $t = 7.9582242 \times 10^{-4}$, where the solution becomes too singular to be resolved by our numerical method. The zoomed-in profiles of $-\omega_1$, $-\psi_1$, and the velocity fields u^r , $-u^z$ are shown in Figure 5. We can see that $-\omega_1$ seems to primarily depend on z and is very flat as a function of r . In Figure 6, we show the curves of important quantities of the solution. At the end of the computation, $\|\omega_1\|_{L^\infty}$ has increased by a factor of around 6.5×10^6 , and $\|\omega\|_{L^\infty}$ has increased by a factor of around 515. We define $(R_1(t), Z_1(t))$ to be the maximum location of $|\omega_1|$. As the solution approaches the potential blow-up, we observe that $R_1(t) = 0$, and $-\omega_1$ becomes essentially one-dimensional. Notice that $Z_1(t)$ decays very fast towards zero, scaling roughly like $(T - t)^c$ with some terminal time T and an exponent $c > 1$.

We also observe that the double logarithm curve $\log \log \|\omega\|_{L^\infty}$ grows superlinear

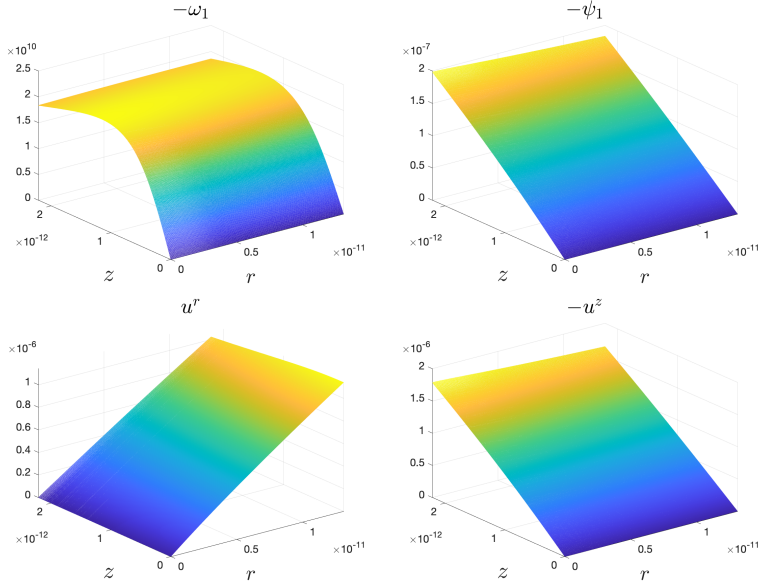


FIG. 5. Zoomed-in 3D profiles of $-\omega_1$, $-\psi_1$, u^r and $-u^z$ at $t = 7.9582242 \times 10^{-4}$ near the origin $(0, 0)$.

in time, which provides the first evidence that the solution may develop a potential singularity in finite time. Another strong evidence is the rapid growth of the time integral $\int_0^t \|\omega(s)\|_{L^\infty} ds$, which may violate the Beale-Kato-Majda non-blow-up criterion.

The kinetic energy E is a conservative quantity for the n -D axisymmetric Euler equations with no swirl. After more than 5.5×10^4 iterations, the relative change in the kinetic energy E is less than 1.17×10^{-4} . The conservation of energy provides additional support for the accuracy of our numerical solution.

3.2. Scaling analysis. In Figure 7, we perform scaling analysis for the potential blow-up. Similar to the 3D case, the scaling invariant property of the n -D Euler equations implies that if the self-similar blow-up exists, then $\|\omega\|_{L^\infty}$ and $\|\psi_{1,z}\|_{L^\infty}$ should scale like $1/(T-t)$, where T is the blow-up time. In the top row of Figure 7, $1/\|\omega\|_{L^\infty}$ or $1/\|\psi_{1,z}\|_{L^\infty}$ as a function of t gives excellent linear fitting with R^2 value higher than 0.9998. The blow-up times estimated by the fitting of these two quantities also match each other very well, with one 8.0134092×10^{-4} and another 8.0134974×10^{-4} . It provides further evidence that the our 10-D Euler equations develop a potential finite-time self-similar singularity.

In the second row of Figure 7, we fit the scaling factors c_l and c_ω from the self-similar relation $\|\omega_1\|_{L^\infty} \sim 1/(T-t)^{c_\omega}$ and $Z_1 \sim (T-t)^{c_l}$. We find the best constant c for $\|\omega\|_{L^\infty}^{-1/c}$ or $Z_1^{1/c}$ such that they achieve the highest R^2 values when fitting with t . Our results give $c_l = 5.75$ and $c_\omega = 3.95$, which satisfies the relation (2.7) $c_\omega = 1 + \alpha c_l$ approximately. Moreover, the estimated blow-up times in both cases agree with each other quite well.

3.3. Dynamic rescaling formulation. The scaling analysis suggests that the potential singularity is very likely to be self-similar. Therefore, we use the dynamic rescaling formulation to study the potential self-similar profile of the solution. The dy-

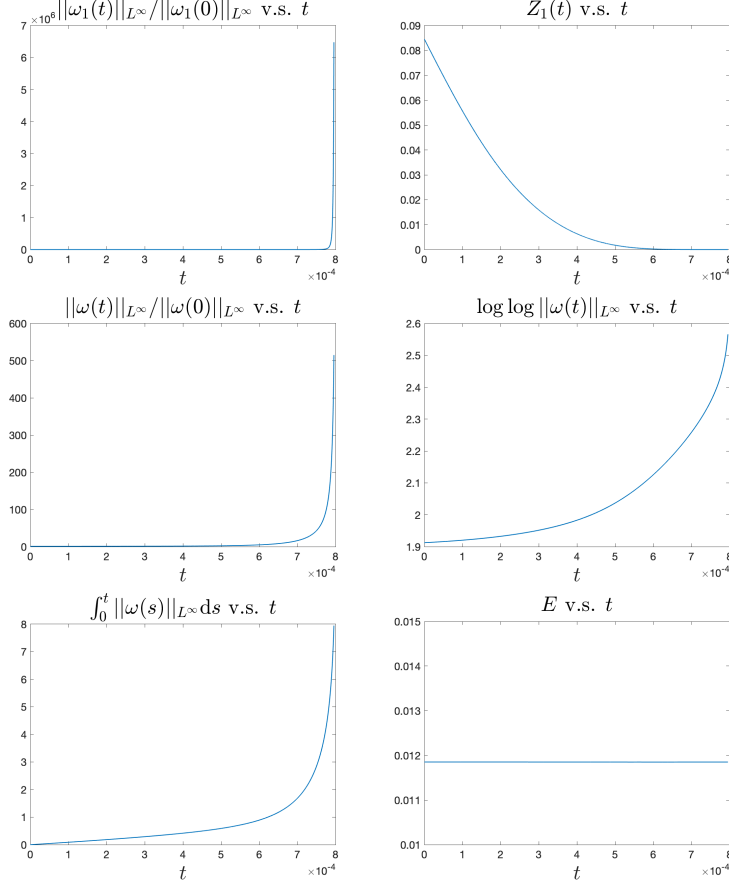


FIG. 6. Curves of $\|\omega_1\|_{L^\infty}$, Z_1 , $\|\omega\|_{L^\infty}$, $\log \log \|\omega\|_{L^\infty}$, $\int_0^t \|\omega(s)\|_{L^\infty} ds$ and E as a function of time.

dynamic rescaling formulation captures the potential self-similar profile by dynamically rescaling the solution to the original equations, and has widely been used in the study of singularity formation of nonlinear Schrödinger equations as in [17, 10, 11, 9, 18], and the 3D Euler equations as in [7, 1, 3, 8].

Similar to Section 4 of [8], the dynamic rescaling formulation in the n -D case becomes

$$(3.1a) \quad \tilde{\omega}_{1,\tau} + (\tilde{c}_l \xi + \tilde{u}^\xi) \tilde{\omega}_{1,\xi} + (\tilde{c}_l \zeta + \tilde{u}^\zeta) \tilde{\omega}_{1,\zeta} = \left(\tilde{c}_\omega - (n-2-\alpha) \tilde{\psi}_{1,\zeta} \right) \tilde{\omega}_1,$$

$$(3.1b) \quad -\tilde{\psi}_{1,\xi\xi} - \tilde{\psi}_{1,\zeta\zeta} - \frac{n}{\xi} \tilde{\psi}_{1,\xi} = \tilde{\omega}_1 \xi^{\alpha-1},$$

$$(3.1c) \quad \tilde{u}^\xi = -\xi \tilde{\psi}_{1,\zeta}, \quad \tilde{u}^\zeta = (n-1) \tilde{\psi}_1 + \xi \tilde{\psi}_{1,\xi}.$$

The solution $\{\tilde{\omega}_1, \tilde{\psi}_1\}$ of (3.1) is related to the solution $\{\omega_1, \psi_1\}$ of (2.4) via the following way:

$$(3.2) \quad \begin{aligned} \tilde{\omega}_1(\xi, \zeta, \tau) &= \tilde{C}_\omega(\tau) \omega_1 \left(\tilde{C}_l(\tau) \xi, \tilde{C}_l(\tau) \zeta, t(\tau) \right), \\ \tilde{\psi}_1(\xi, \zeta, \tau) &= \tilde{C}_\psi(\tau) \psi_1 \left(\tilde{C}_l(\tau) \xi, \tilde{C}_l(\tau) \zeta, t(\tau) \right), \end{aligned}$$

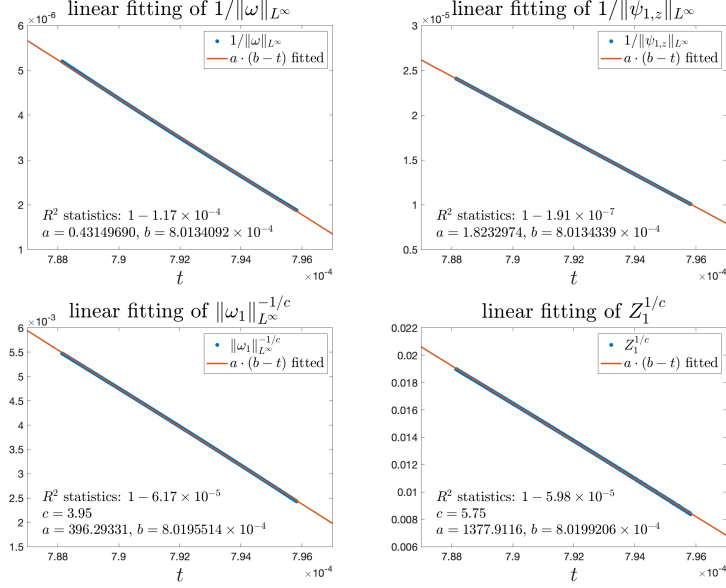


FIG. 7. Fitting the scales of $\|\omega\|_{L^\infty}$, $\|\psi_{1,z}\|_{L^\infty}$, and $\|\omega_1\|_{L^\infty}$, Z_1 .

where we define $\tilde{c}_\psi(\tau) = \tilde{c}_\omega(\tau) + (1 + \alpha)\tilde{c}_l(\tau)$ and

$$\begin{aligned}\tilde{C}_\omega(\tau) &= \exp\left(\int_0^\tau \tilde{c}_\omega(s)ds\right), & \tilde{C}_\psi(\tau) &= \exp\left(\int_0^\tau \tilde{c}_\psi(s)ds\right), \\ \tilde{C}_l(\tau) &= \exp\left(-\int_0^\tau \tilde{c}_l(s)ds\right), & t'(\tau) &= \tilde{C}_\psi(\tau)\tilde{C}_l(\tau) = \tilde{C}_\omega(\tau)\tilde{C}_l^{-\alpha}(\tau).\end{aligned}$$

We choose the scaling parameters $\{\tilde{c}_l(\tau), \tilde{c}_\omega(\tau)\}$ in (3.1) to satisfy the following normalization conditions imposed by us

$$(3.3) \quad \tilde{\omega}_1(0, 1, \tau) = -1, \quad \tilde{\omega}_{1,\zeta}(0, 1, \tau) = 0, \quad \text{for } \tau \geq 0.$$

When (3.1) converges to a steady state, the scaling factors $\{c_l, c_\omega\}$ in (2.5) can be derived from the scaling parameters $\{\tilde{c}_l, \tilde{c}_\omega\}$ via

$$(3.4) \quad c_l = -\frac{\tilde{c}_l}{\tilde{c}_\omega + \alpha\tilde{c}_l}, \quad c_\omega = \frac{\tilde{c}_\omega}{\tilde{c}_\omega + \alpha\tilde{c}_l}, \quad c_\psi = \frac{\tilde{c}_\psi}{\tilde{c}_\omega + \alpha\tilde{c}_l}.$$

We use the operator splitting method described in [8] to solve (3.1) with the normalization conditions (3.3). We observe fast convergence to the steady state using the solution from the last iteration of the adaptive mesh method as the initial condition for the dynamic rescaling formulation. In Figure 8, we plot the relative time derivative strength $\|\tilde{\omega}_{1,\tau}(\tau)\|_{L^\infty}/\|\tilde{\omega}_1(\tau)\|_{L^\infty}$. This relative strength of the time derivative has a decreasing trend and goes down below 1.78×10^{-6} near the end of the computation, which provides strong evidence that we are close to the steady state.

In Figure 9, we plot the curves of the scaling factors. In the top row, the scaling factors \tilde{c}_l , \tilde{c}_ω that are used in the dynamic rescaling formulation demonstrate good convergence to a constant value. In the second row, the scaling factors c_l , c_ω that appear in the self-similar ansatz converge to the value of 5.897 and 3.949 respectively.

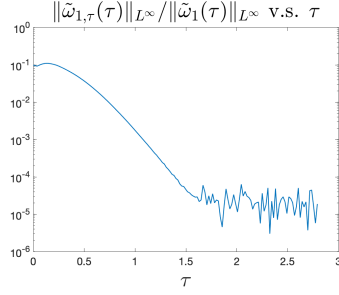


FIG. 8. Curve of the relative time derivative strength $\|\tilde{\omega}_{1,\tau}(\tau)\|_{L^\infty} / \|\tilde{\omega}_1(\tau)\|_{L^\infty}$.

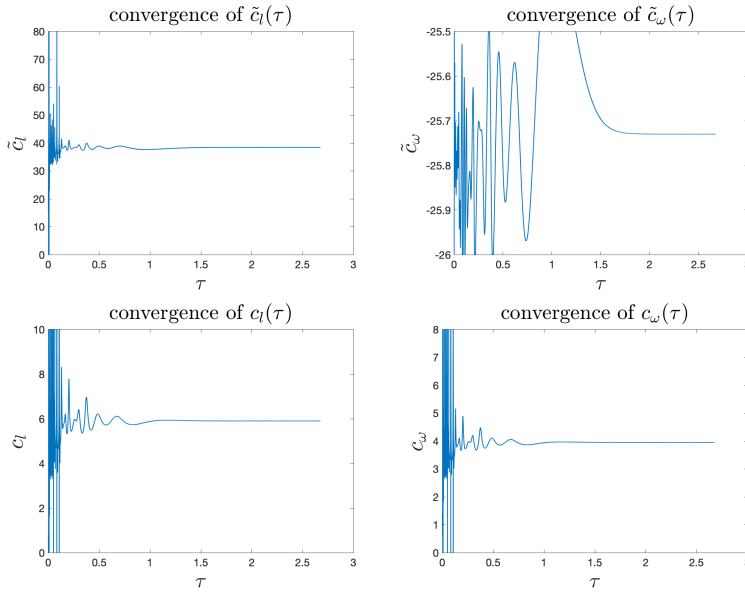


FIG. 9. Convergence curves of the scaling factors using dynamic rescaling method. Top row: \tilde{c}_l ; and \tilde{c}_ω . Bottom row: c_l and c_ω .

The estimated values for c_l , c_ω not only match the estimated values from the scaling analysis, but also satisfy the relation $c_\omega = 1 + \alpha c_l$ approximately. This provides another verification of the validity of our results.

The steady states of $-\tilde{\omega}_1$ and $-\tilde{\psi}_1$ are plotted in Figure 10. We can see that $-\tilde{\omega}_1$ is very close to be one-dimensional, with little tilt towards $\xi = 0$.

4. Hölder exponent, anisotropic scaling, and dimension in the potential self-similar blow-up. In this section, we explore how the Hölder exponent α , the anisotropic scaling parameter δ , which will soon be introduced, and the dimension n influence the blow-up of the n -D Euler equations. In Question 7 of [5], the authors raised the question whether the n -D axisymmetric Euler equations with no swirl would form a finite-time singularity from smooth initial data when $n \geq 4$. While we cannot provide direct numerical evidence to this equation, our results show that it is very likely that the n -D axisymmetric Euler equations with no swirl can form singularity in finite-time if the initial vorticity is C^α with $\alpha < 1 - \frac{2}{n}$. We can see that as n grows

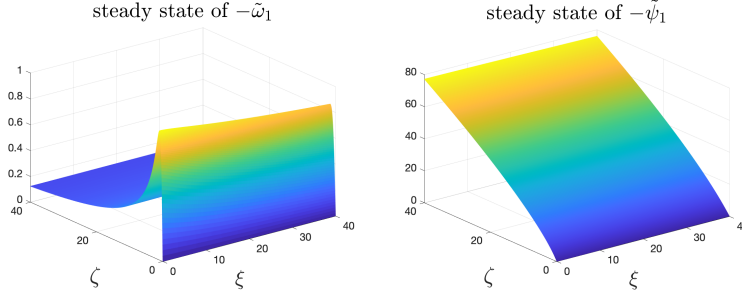


FIG. 10. Steady states of $-\tilde{\omega}_1$ and $-\tilde{\psi}_1$, with $n = 10$ and $\alpha = 0.5$.

large, there is a wider range of initial data that admits finite-time blow-up. Due to our design of the initial data, in the limit case $n \rightarrow +\infty$ the regularity of the initial data will become almost Lipschitz.

Similar to Section 5 of [8], we stretch the physical domain $\mathcal{D} = [0, 1] \times [0, \frac{1}{2}]$ to $\mathcal{D}_\delta = [0, 1] \times [0, \frac{1}{2\delta}]$, and stretch the initial data $\omega_1^\circ(r, z)$ to $\omega_1^\circ(r, \delta z)$. Here δ is the anisotropic parameter controlling the stretch or squeeze. The case of $\delta = 1$ corresponds to no stretch and $\delta < 1$, $\delta > 1$ correspond to stretch and squeeze, respectively. Instead of redefining the physical domain \mathcal{D} and the initial data (2.12), we define the new variables

$$(4.1) \quad \hat{\omega}_1(r, z, t) = \omega_1(r, z/\delta, t/\delta), \quad \hat{\psi}_1(r, z, t) = \psi_1(r, z/\delta, t/\delta).$$

Since it does not cause much ambiguity, we still use the symbol ω_1 and ψ_1 to represent $\hat{\omega}_1$ and $\hat{\psi}_1$ afterwards. With the newly defined variables, the axisymmetric n -D Euler equations with no swirl are equivalent to

$$(4.2a) \quad \omega_{1,t} + u^r \omega_{1,r} + u^z \omega_{1,z} = -(n-2-\alpha)\psi_{1,z}\omega_1,$$

$$(4.2b) \quad -\psi_{1,rr} - \delta^2 \psi_{1,zz} - \frac{n}{r} \psi_{1,r} = \omega_1 r^{\alpha-1},$$

$$(4.2c) \quad u^r = -r\psi_{1,z}, \quad u^z = (n-1)\psi_1 + r\psi_{1,r}.$$

And as a result, the physical domain \mathcal{D} and the initial data (2.12) remain formally unchanged. Comparing (2.4) and (4.2), the only difference is the coefficient before $\psi_{1,zz}$ the Poisson equation of ψ_1 .

In the following, for each combination of α , δ and n , we first use the adaptive mesh method to solve the equations (4.2) close enough to its possible blow-up time, and then use the dynamic rescaling formulation to continue the computation and capture the potential self-similar structure.

In Figures 11 and 12, we provide the cross sections of the steady states $-\tilde{\omega}_1$ and $-\tilde{\psi}_1$ for different α when $n = 10$ and $\delta = 1.0$. We can see that as α increases, the steady state becomes flatter in ξ . The cross-section in ζ shows the different decay rates for different values of α . It is also very interesting to see that the ζ -cross section of $-\tilde{\psi}_1$ seems to be well approximated by a linear function of ζ . In fact, this phenomenon will become even clearer in the discussion in the next section.

In Figures 13 and 14, we provide the cross sections of the steady states $-\tilde{\omega}_1$ and $-\tilde{\psi}_1$ for different δ when $n = 10$ and $\alpha = 0.5$. We have the following observations:

- the ξ -cross section of $-\tilde{\omega}_1$ seems to become flat in ξ as δ decreases, which seems to imply that as $\delta \rightarrow 0$, $-\tilde{\omega}_1$ will be a function of ζ only,

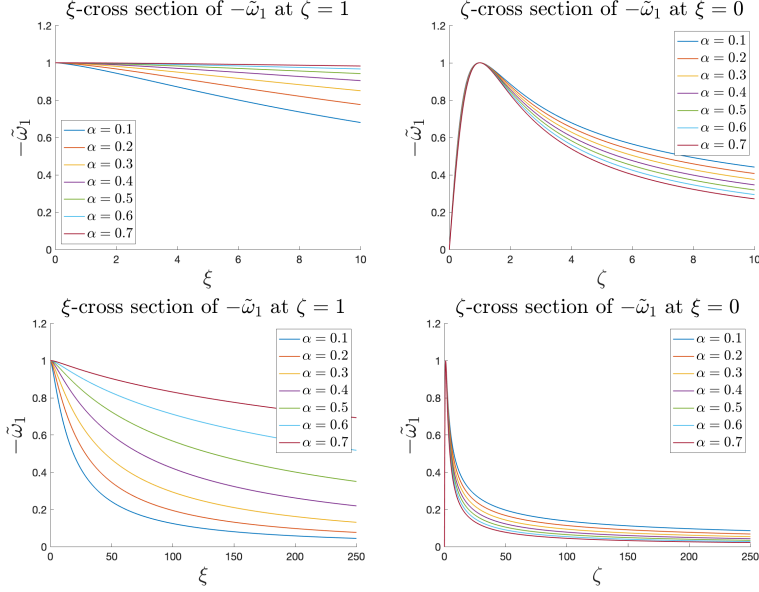


FIG. 11. Cross sections of steady states of $-\tilde{\omega}_1$ with different α with $\delta = 1.0$ in \mathbb{R}^{10} . Top row: on a local window. Bottom row: on a larger window.

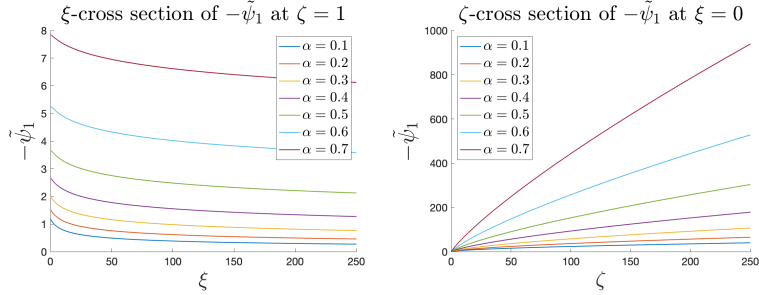


FIG. 12. Cross sections of steady states of $-\tilde{\psi}_1$ with different α with $\delta = 1.0$ in \mathbb{R}^{10} .

- the ζ -cross section of $-\tilde{\omega}_1$ seems to be insensitive to the choice of δ ,
- the scale of $-\tilde{\psi}_1$ seems to grow drastically as δ decreases, and the ζ -cross section of $-\tilde{\psi}_1$ seems to be linear in ζ as δ approaches zero.

The above observation motivates our model for the blow-up mechanism in Section 5.

Moreover, we list the scaling factors for different combination of α and δ in Table 1. The empty cells refer to the situation where we do not observe a potential finite time blow-up for that particular pair of parameters. We observe that c_l monotonically increases with α and δ . When α and δ are approaching the critical values between the blow-up and non-blow-up, c_l becomes extremely large. In Figure 15, we visualize the data by plotting $1/c_l$ against α , both for the \mathbb{R}^3 case and the \mathbb{R}^{10} case. As δ tends to zero, the relation between $1/c_l$ and α becomes more and more linear. In fact, we conjecture that it may approach the green dash line as δ approaches zero. We remark that the green dash line corresponds to a limiting relationship between c_l and α that we conjecture to hold as $\delta \rightarrow 0$. More specifically, we conjecture the following scaling

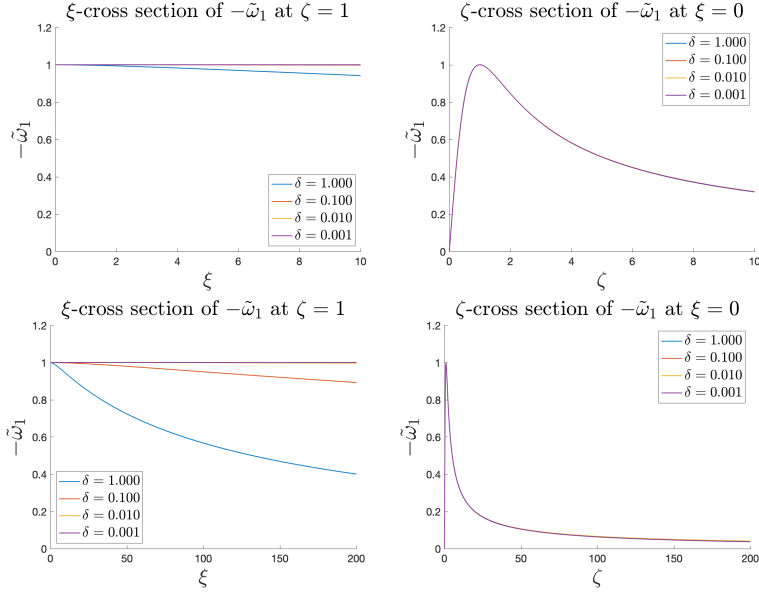


FIG. 13. Cross sections of steady states of $-\tilde{\omega}_1$ with different δ with $\alpha = 0.5$ in \mathbb{R}^{10} . Top row: on a local window. Bottom row: on a larger window.

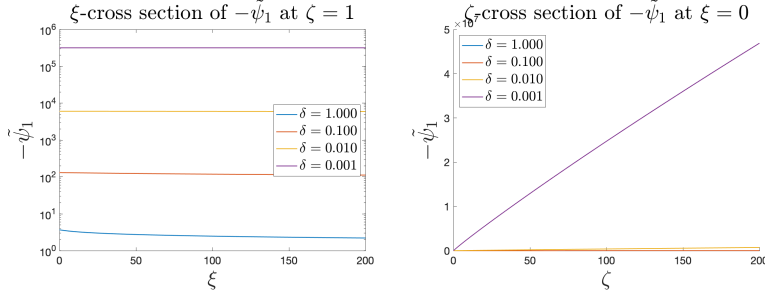


FIG. 14. Cross sections of steady states of $-\tilde{\psi}_1$ with different δ with $\alpha = 0.5$ in \mathbb{R}^{10} . Notice that the left figure has a logarithmic y-axis.

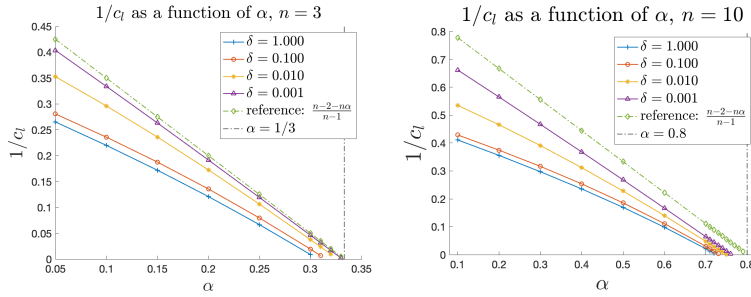


FIG. 15. $1/c_l$ as a function of α , with the guessed limit (in green) for $\delta = 0$.

relationships for c_l and c_ω as $\delta \rightarrow 0$:

$$(4.3) \quad c_l = \frac{n-1}{n-2-n\alpha}, \quad c_\omega = \frac{n-2-\alpha}{n-2-n\alpha}.$$

c_l		δ			
		10^0	10^{-1}	10^{-2}	10^{-3}
α	0.10	2.432	2.330	1.869	1.511
	0.20	2.811	2.670	2.148	1.770
	0.30	3.363	3.160	2.557	2.141
	0.40	4.244	3.939	3.207	2.717
	0.50	5.897	5.384	4.385	3.732
	0.60	10.16	8.989	7.149	5.996
	0.70	47.14	33.14	20.95	15.50
	0.71	76.10	46.07	26.10	18.44
	0.72	199.8	75.89	34.65	22.77
	0.73	-	218.2	51.63	29.75
	0.74	-	-	101.6	42.93
	0.75	-	-	3539	77.13
	0.76	-	-	-	381.0

TABLE 1
The scaling factor c_l in \mathbb{R}^{10} for different choice of α and δ .

We will provide some formal derivation of this relationship in Section 5. In both cases with $n = 3$ and $n = 10$, it seems very likely that the curve of $1/c_l$ will become the green dash line in the limit as $\delta \rightarrow 0$. The intersection of the green dash line and the α axis is exactly $1 - \frac{2}{n}$, suggesting that $c_l \rightarrow +\infty$.

At the end of this section, we also study how the dimension n influences the finite-time blow-up. We fix $\alpha = 0.1$ and $\delta = 1$, and try different choices of dimensions $n = 3, 4, 5, 6, 8, 10$ using the same initial data (2.12).

In Table 2, we report the estimated blow-up times T and scaling factors c_l for different dimensions. It is not surprising that the blow-up time of the same initial data is shorter for the higher dimensional case, because the vortex stretching term has a larger amplification coefficient. However, the scaling factor c_l is smaller for larger n . Intuitively, the velocity component u^z seems to be stronger with larger n . This phenomenon suggests that in the high dimensional case, the dimension-related term $-\frac{n}{r}\partial_r$ in the Poisson equation controls ψ_1 and therefore weakens the collapsing speed of the solution. We also remark that the decay of c_l with n significantly slows down in Table 2. It is tempting to speculate if there is a limit of c_l as n approaches infinity.

In Figure 16 and 17, we provide the cross sections of the steady states of $-\tilde{\omega}_1$ and $-\tilde{\psi}_1$ from the dynamic rescaling formulation. We observe that the cross sections change with n . But as n becomes larger than 5, the difference quickly narrows down. This would give more evidence that there is some non-trivial limit as n goes to infinity. It would be very interesting to further explore this infinite dimension limit in the future.

n	3	4	5	6	8	10
$10^4 \times T$	4.183	3.589	2.877	2.498	2.089	1.866
c_l	4.549	3.218	2.851	2.680	2.514	2.432

TABLE 2
Estimated blow-up times T and scaling factors c_l in different dimensions with $\alpha = 0.1$, $\delta = 1$.

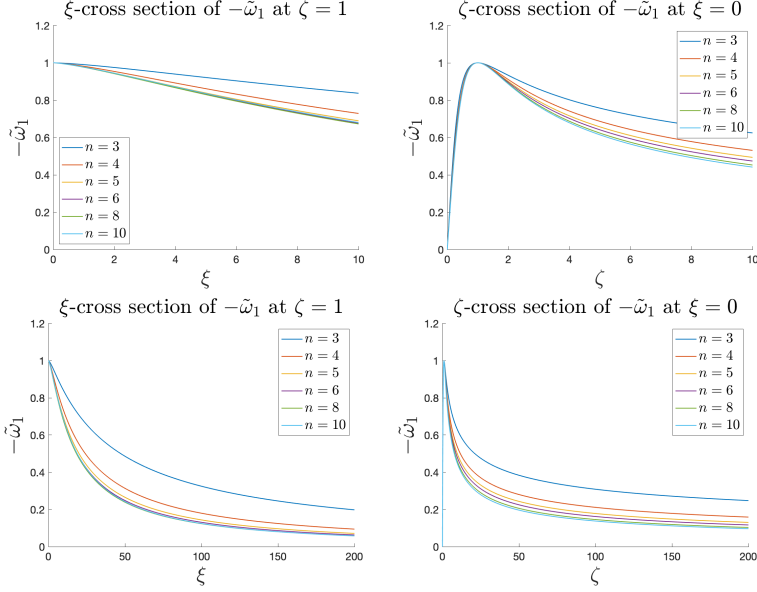


FIG. 16. Cross sections of steady states of $-\tilde{\omega}_1$ with different n with $\alpha = 0.1$, $\delta = 1$. Top row: on a local window. Bottom row: on a larger window.

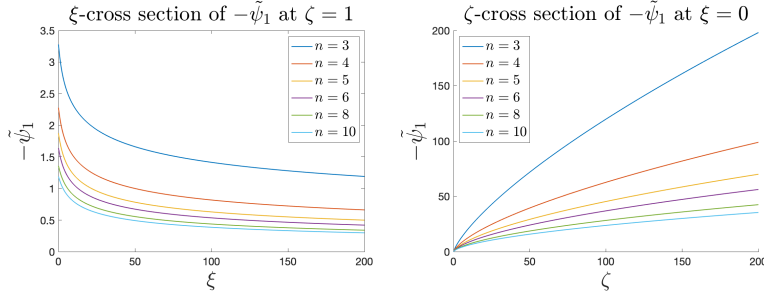


FIG. 17. Cross sections of steady states of $-\tilde{\psi}_1$ with different n with $\alpha = 0.1$, $\delta = 1$.

5. Possible mechanism of the potential singularity formation. Currently, there is a lack of mathematical analysis to explain the numerical phenomenon presented in Section 3 and Section 4. Therefore, we dig deep into the potential blow-up solutions and provide some understanding of the singularity formation mechanism.

5.1. The limit of $\delta \rightarrow 0$. To begin with, we can see from Figure 15 that for any $\delta > 0$, c_l increases with α , and seems to approach infinity at some critical value, which we denote as α^* . In both cases ($n = 3$ and $n = 10$), α^* increases and seems to approach $1 - \frac{2}{n}$ as δ tends to zero. In our numerical experiments, the value of α^* seems to divide the solutions of the n -D Euler equations in three categories. For $\alpha < \alpha^*$, we observe potential self-similar blow-up in finite-time; for $\alpha > \alpha^*$, we have strong evidence that there is no finite-time blow-up; and for $\alpha = \alpha^*$, it is hard to determine whether the solution blows up in finite time, because the quantities are of critical state. The above phenomenon suggests the following conjecture, which can be viewed as a high-dimensional generalization of Conjecture 8 of [5]:

CONJECTURE 5.1. *For any $\alpha < 1 - \frac{2}{n}$, there exist C_c^α initial vorticity such that the n -D axisymmetric Euler equations with no swirl develop singularity in finite time.*

In addition, the numerical phenomenon highlights the importance of the limiting case of $\delta \rightarrow 0$, because in our scenario, this limit gives the widest range of α that admits potential finite-time blow-up. Therefore, it would be very interesting to study the limit of $\delta \rightarrow 0$.

5.2. One-dimensional structure at $\xi = 0$. It is important to note from Figure 13 that the profile of $-\tilde{\omega}_1$ tends to become one-dimensional, and the maximum of $-\tilde{\omega}_1$ always locates at $\xi = 0$. Therefore, the cross sections of $-\tilde{\omega}_1$ at $\xi = 0$ can be used to characterize the profile of $-\tilde{\omega}_1$. In the dynamic rescaling formulation (3.1), we restrict $\xi = 0$, and use $\tilde{\Omega}_1, \tilde{\Psi}_1$ to represent the ζ -cross section of the steady states $\tilde{\omega}_1, \tilde{\psi}_1$:

$$\tilde{\Omega}_1(\zeta, \tau) = \tilde{\omega}_1(0, \zeta, \tau), \quad \tilde{\Psi}_1(\zeta, \tau) = \tilde{\psi}_1(0, \zeta, \tau).$$

Note that the time dependence in fact disappears here. We reduce (3.1a) to the following equation for $\tilde{\Omega}_1$:

$$(5.1) \quad \tilde{\Omega}_{1,\tau} + \left(\tilde{c}_i \zeta + (n-1)\tilde{\Psi}_1 \right) \tilde{\Omega}_{1,\zeta} = \left(\tilde{c}_\omega - (n-2-\alpha)\tilde{\Psi}_{1,\zeta} \right) \tilde{\Omega}_1.$$

To close the system, we also need to derive a reduced Biot-Savart law along $\xi = 0$.

5.3. Asymptotic Expansion of $\tilde{\Omega}_1$ and $\tilde{\Psi}_1$. In the limiting case of $\delta \rightarrow 0$, we look for an asymptotic expansion of $\tilde{\Psi}_1$ as the solution to the Poisson equation. To this end, we assume the following expansion of $\tilde{\Omega}_1, \tilde{\Psi}_1$ in the near field of ζ close to zero:

$$(5.2a) \quad \tilde{\Omega}_1(\zeta) = \sum_{k=0}^{+\infty} \lambda_{2k+1}(\delta) \zeta^{2k+1} = \lambda_1(\delta) \zeta^1 + \lambda_3(\delta) \zeta^3 + \lambda_5(\delta) \zeta^5 + \dots,$$

$$(5.2b) \quad \tilde{\Psi}_1(\zeta) = \sum_{k=0}^{+\infty} \kappa_{2k+1}(\delta) \zeta^{2k+1} = \kappa_1(\delta) \zeta^1 + \kappa_3(\delta) \zeta^3 + \kappa_5(\delta) \zeta^5 + \dots.$$

Note that here we only keep the odd terms, because the symmetry assumption guarantees that $\tilde{\Omega}_1, \tilde{\Psi}_1$ are odd functions of ζ . The parameter δ controls the coefficients of the expansion, and thus influences the singularity formation of the n -D Euler equations.

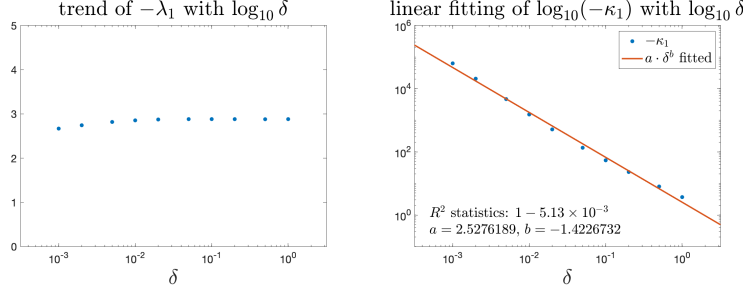
We then use numerical methods to study the dependence of the coefficients on δ . For the first-order coefficients $\lambda_1(\delta)$ and $\kappa_1(\delta)$, we have

$$\lambda_1(\delta) = \tilde{\Omega}_{1,\zeta}(0), \quad \kappa_1(\delta) = \tilde{\Psi}_{1,\zeta}(0).$$

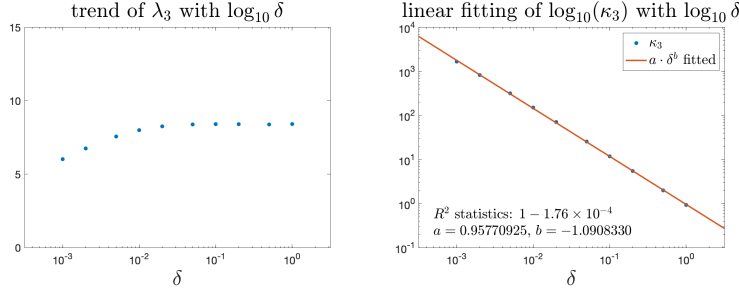
In Figure 18, we set $n = 3$, $\alpha = 0.1$, and use $\delta \in \{0.001, 0.002, 0.005, 0.01, 0.02, 0.05, 0.1, 0.2, 0.5, 1.0\}$ to study the relation of λ_1, κ_1 with respect to δ . We can see that λ_1 seems to remain at a constant scale for this wide range of δ . This is consistent with the observation in Section 4 that the ζ -cross section of $-\tilde{\omega}_1$ seems to be insensitive to the value of δ . This suggests that $\lambda_1 = O(1)$ as $\delta \rightarrow 0$. We can also see there is a clear linear relation, up to some perturbation, between $\log_{10} \delta$ and $\log_{10}(-\kappa_1)$. The linear fitting suggests that $\kappa_1 = O(\delta^{-1.423})$ as $\delta \rightarrow 0$.

As for the third-order coefficients $\lambda_3(\delta)$ and $\kappa_3(\delta)$, we similarly have

$$\lambda_3(\delta) = \frac{1}{6} \tilde{\Omega}_{1,\zeta\zeta\zeta}(0), \quad \kappa_3(\delta) = \frac{1}{6} \tilde{\Psi}_{1,\zeta\zeta\zeta}(0).$$

FIG. 18. The relation of λ_1, κ_1 with δ , when $n = 3$ and $\alpha = 0.1$.

In Figure 19, we study the relation of λ_3, κ_3 with respect to δ . Again, λ_3 remains at a constant scale for different values of δ that we computed. And $\log_{10}(\kappa_3)$ has a linear relation with $\log_{10} \delta$. Our study seems to suggest that $\lambda_3 = O(1)$ and $\kappa_3 = O(\delta^{-1.091})$ as $\delta \rightarrow 0$. We remark that although the numerical implementation of the third-order derivative introduces larger errors, we still think κ_3 is a lower order term as compared to κ_1 . In Table 3, we fit the linear model $\tilde{\Psi}_1 \sim b\zeta$ with no intercept term, for $\zeta \in [0, 1000]$. We can clearly see that as δ approaches zero, the R^2 of the linear fitting increases, which implies that the first-order term $\kappa_1(\delta)\zeta$ indeed dominates other terms in the expansion of $\tilde{\Psi}_1$.

FIG. 19. The relation of λ_3, κ_3 with δ , when $n = 3$ and $\alpha = 0.1$.

δ	1.0	0.5	0.2	0.1	0.05
$1 - R^2$	5.00×10^{-2}	4.42×10^{-2}	2.82×10^{-2}	1.49×10^{-2}	6.18×10^{-3}

δ	0.02	0.01	0.005	0.002	0.001
$1 - R^2$	1.65×10^{-3}	6.59×10^{-4}	3.53×10^{-4}	2.99×10^{-4}	1.67×10^{-4}

TABLE 3

R^2 of the fitting of $\tilde{\Psi}_1$ and ζ with no intercept term for $0 \leq \zeta \leq 1000$.

As for the higher-order terms, we expect $\lambda_{2k+1} = O(1)$ because $\tilde{\Omega}_1$ seems to be insensitive with δ as shown in Figure 13. We also expect κ_{2k+1} to be lower order terms of κ_1 for $k \geq 1$, because we can see in Table 3, the linear fitting of $\tilde{\Psi}_1$ improves as δ decreases in a very wide range $\zeta \in [0, 1000]$.

In summary, we tend to believe that for the asymptotic expansion (5.2), the coefficients have the following properties:

- $\lambda_{2k+1} = O(1)$ as $\delta \rightarrow 0$, for $k \geq 0$,
- $\kappa_{2k+1}/\kappa_1 \rightarrow 0$ as $\delta \rightarrow 0$, for $k \geq 1$. In other words, the leading order expansion for $\tilde{\Psi}_1$ is $\tilde{\Psi}_1 \approx \kappa_1(\delta)\zeta$.

5.4. Scaling Factors of the Self-Similar Profile. With the asymptotic expansion we obtained above, we turn to (5.1). In the steady state, the time derivative disappears, and we should have

$$(5.3) \quad \left(\tilde{c}_l \zeta + (n-1)\tilde{\Psi}_1 \right) \tilde{\Omega}_{1,\zeta} = \left(\tilde{c}_\omega - (n-2-\alpha)\tilde{\Psi}_{1,\zeta} \right) \tilde{\Omega}_1.$$

Now we plug in the asymptotic expansion (5.2), and compare the coefficients of the first two non-zero orders to get

$$(5.4) \quad \lambda_1 (\tilde{c}_l + (n-1)\kappa_1) = \lambda_1 (\tilde{c}_\omega - (n-2-\alpha)\kappa_1),$$

$$(5.5) \quad 3\lambda_3 (\tilde{c}_l + (n-1)\kappa_1) + (n-1)\lambda_1\kappa_3 = \lambda_3 (\tilde{c}_\omega - (n-2-\alpha)\kappa_1) - 3(n-2-\alpha)\lambda_1\kappa_3.$$

Now we consider the limit of $\delta \rightarrow 0$. Since κ_1 is the more dominating term than κ_3 , and $\lambda_{2k+1} = O(1)$, the leading order terms of (5.5) need to cancel each other, which implies that

$$(5.6) \quad 3\lambda_3 (\tilde{c}_l + (n-1)\kappa_1) = \lambda_3 (\tilde{c}_\omega - (n-2-\alpha)\kappa_1).$$

We can see from Figure 18, $\lambda_1(\delta)$ does not approach zero as $\delta \rightarrow 0$. If we further assume that λ_3 does not approach zero either as $\delta \rightarrow 0$, we conclude from (5.4) and (5.6) that the following relationship must hold true:

$$\tilde{c}_l = -(n-1)\kappa_1, \quad \tilde{c}_\omega = (n-2-\alpha)\kappa_1.$$

As a consequence, at the limit $\delta \rightarrow 0$, (3.4) implies that

$$(5.7) \quad c_l = -\frac{1}{\tilde{c}_\omega/\tilde{c}_l + \alpha} = \frac{n-1}{n-2-n\alpha}, \quad c_\omega = \frac{\tilde{c}_\omega/\tilde{c}_l}{\tilde{c}_\omega/\tilde{c}_l + \alpha} = \frac{n-2-\alpha}{n-2-n\alpha}.$$

The above limit seems to match pretty well with our numerical results. In Figure 15, we plot this scaling relationship in green. In both $n = 3$ and $n = 10$ cases, the numerical estimate for c_l seems to move toward the green line as δ approaches zero. We also remark that for the prediction of c_l , $\alpha = 1 - \frac{2}{n}$ is the upper bound to guarantee c_l to remain positive, which is required by a self-similar focusing singularity. This value is consistent with our numerical observation, as concluded in Conjecture 5.1.

We state our second conjecture in this section below:

CONJECTURE 5.2. *For any $\alpha < 1 - \frac{2}{n}$, if δ is small enough, the n -dimensional axisymmetric Euler equations with no swirl and with initial data (2.12) will develop a self-similar singularity in finite time. When $\delta \rightarrow 0$, the scaling factor c_l of the self-similar ansatz (2.5) will converge to $\frac{n-1}{n-2-n\alpha}$.*

We remark that the above formal analysis does not provide direct information on the self-similar profile. Such information would require high-order information in the expansion.

6. A one-dimensional model for the potential self-similar blow-up. We observe that as δ decreases, $-\tilde{\omega}_1$ will become extremely flat in ξ , and we believe in the $\delta \rightarrow 0$ limit, $-\tilde{\omega}_1$ will eventually become a function of ζ only in a relatively large domain. Based on this observation, we assume that

$$\omega_1(r, z) = \omega_1(0, z),$$

and derive a one-dimensional model for the n -D Euler equations.

At $r = 0$, the velocity fields (2.4c) become $u^r = 0$, $u^z = (n-1)\psi_1$. Therefore, the vorticity equation (2.4a) becomes

$$\omega_{1,t}(0, z) + (n-1)\psi_1(0, z)\omega_{1,z}(0, z) = -(n-2-\alpha)\psi_{1,z}(0, z)\omega_1(0, z).$$

As for the Poisson equation (2.4b), we use the Green's function $G_{n,\alpha,\delta}(r, r', z, z')$ for the operator $L_{n,\alpha,\delta} = r^{1-\alpha}(-\partial_{rr} - \frac{n}{r}\partial_r - \delta^2\partial_{zz})$. We have

$$\begin{aligned} \psi_1(r, z) &= \int_{(r', z') \in \mathcal{D}} G_{n,\alpha,\delta}(r, r', z, z')\omega_1(r', z')dr'dz', \\ &= \int_{(r', z') \in \mathcal{D}} G_{n,\alpha,\delta}(r, r', z, z')\omega_1(0, z')dr'dz', \end{aligned}$$

and therefore

$$\psi_1(0, z) = \int_0^{1/2} H_{n,\alpha,\delta}(z, z')\omega_1(0, z')dz',$$

where

$$H_{n,\alpha,\delta}(z, z') = \int_0^1 G_{n,\alpha,\delta}(0, r', z, z')dr'.$$

Putting these equations together, and omitting the r -coordinate when there is no ambiguity, we have the following closed system in 1D: for $z \in [0, 1/2]$, ω_1 and ψ_1 are functions of z whose evolution in time is governed by the equations

$$(6.1a) \quad \omega_{1,t} + (n-1)\psi_1\omega_{1,z} = -(n-2-\alpha)\psi_{1,z}\omega_1,$$

$$(6.1b) \quad \psi_1 = T_{n,\alpha,\delta}\omega_1,$$

where $T_{n,\alpha,\delta}$ is an integral transform with kernel function $H_{n,\alpha,\delta}$:

$$T_{n,\alpha,\delta}\omega_1 = \int_0^{1/2} H_{n,\alpha,\delta}(z, z')\omega_1(z')dz'.$$

6.1. The Kernel Function $H_{n,\alpha,\delta}$. We look for a more explicit expression for the kernel $H_{n,\alpha,\delta}$.

We first undo the change-of-variable (4.1) that stretches the z -direction, and work on the equation

$$-\psi_{1,rr} - \psi_{1,zz} - \frac{n}{r}\psi_{1,r} = \omega_1 r^{\alpha-1},$$

using the original r and z variables with $z \in [0, \frac{1}{2\delta}]$.

Following the idea in [7], we view

$$-\partial_{rr} - \frac{n}{r}\partial_r - \partial_{zz},$$

as the Laplacian operator in the $(n+2)$ -dimensional space for axisymmetric functions. The fundamental solution for the $(n+2)$ -dimensional Laplace equation is

$$\Phi_0(x) = \frac{\Gamma(n/2)}{4\pi^{n/2+1}} \frac{1}{|x|^n},$$

for $x \in \mathbb{R}^{n+2}$.

Now, since we have zero Dirichlet boundary conditions at $r = 1$, $z = 0$, $z = 1/2\delta$, we can obtain the Green's function for the above equation by properly symmetrizing the fundamental solution of the Laplace equation. Finally we redo the change-of-variable (4.1) and get

$$\begin{aligned} G_{n,\alpha,\delta}(r, r', z, z') = & \frac{1}{\delta} \sum_{m \in \mathbb{Z}} \left(G_{n,\alpha} \left(r, r', \frac{z+m}{\delta}, \frac{z'}{\delta} \right) - G_{n,\alpha} \left(r, r', \frac{-z+m}{\delta}, \frac{z'}{\delta} \right) \right. \\ & \left. - G_{n,\alpha} \left(1, rr', \frac{z+m}{\delta}, \frac{z'}{\delta} \right) + G_{n,\alpha} \left(1, rr', \frac{-z+m}{\delta}, \frac{z'}{\delta} \right) \right), \end{aligned}$$

where

$$G_{n,\alpha}(r, r', z, z') = \frac{2^{n-2}}{\pi} \frac{\Gamma(n/2)^2}{\Gamma(n)} \frac{r'^{n+\alpha-1}}{A^{n/2}} {}_2F_1(n/2, n/2, n, B),$$

with Γ being the Gamma function, ${}_2F_1$ being the Gauss hypergeometric function, and

$$A = (r + r')^2 + (z - z')^2, \quad B = 4rr'/A.$$

In fact, it is easy to check that $G_{n,\alpha,\delta}$ satisfies the boundary conditions:

$$G_{n,\alpha,\delta}(1, r', z, z') = G_{n,\alpha,\delta}(r, r', 0, z') = G_{n,\alpha,\delta}(r, r', 1/2, z') = 0.$$

We notice that the Gaussian hypergeometric function ${}_2F_1$ has the property that ${}_2F_1(n/2, n/2, n, 0) = 1$. Therefore, we know that

$$G_{n,\alpha}(0, r', z, z') = \frac{2^{n-2}}{\pi} \frac{\Gamma(n/2)^2}{\Gamma(n)} \frac{r'^{n+\alpha-1}}{(r'^2 + (z - z')^2)^{n/2}},$$

$$G_{n,\alpha}(1, 0, z, z') = 0.$$

And thus we have

$$\begin{aligned} G_{n,\alpha,\delta}(0, r', z, z') = & \frac{2^{n-2}}{\pi} \frac{\Gamma(n/2)^2}{\Gamma(n)} \sum_{m \in \mathbb{Z}} \left(\frac{\delta^{n-1} r'^{n+\alpha-1}}{(\delta^2 r'^2 + (z + m - z')^2)^{n/2}} - \frac{\delta^{n-1} r'^{n+\alpha-1}}{(\delta^2 r'^2 + (z - m + z')^2)^{n/2}} \right). \end{aligned}$$

Finally, we arrive at an expression for $H_{n,\alpha,\delta}$:

$$\begin{aligned} H_{n,\alpha,\delta}(z, z') = & \frac{2^{n-2}}{\pi} \frac{\Gamma(n/2)^2}{\Gamma(n)} \\ & \frac{1}{\delta^{1+\alpha}} \int_0^\delta \sum_{m \in \mathbb{Z}} \left(\frac{r^{n+\alpha-1}}{(r^2 + (z + m - z')^2)^{n/2}} - \frac{r^{n+\alpha-1}}{(r^2 + (z - m + z')^2)^{n/2}} \right) dr. \end{aligned}$$

From $H_{n,\alpha,\delta}$, we can also find the integral transform for $\psi_{1,z}$:

$$\psi_{1,z}(z) = \int_0^{1/2} \partial_z H_{n,\alpha,\delta}(z, z') \omega_1(z') dz',$$

with

$$\partial_z H_{n,\alpha,\delta}(z, z') = \frac{n2^{n-2} \Gamma(n/2)^2}{\pi \Gamma(n)}$$

$$\frac{1}{\delta^{1+\alpha}} \int_0^\delta \sum_{m \in \mathbb{Z}} \left(\frac{r^{n+\alpha-1} (z+m-z')}{(r^2 + (z+m-z')^2)^{n/2+1}} - \frac{r^{n+\alpha-1} (z-m+z')}{(r^2 + (z-m+z')^2)^{n/2+1}} \right) dr.$$

We remark that for z, z' such that $z - z' \notin \mathbb{Z}$, we have $H_{n,\alpha,\delta}(z) \rightarrow \infty$ as $\delta \rightarrow 0$. This matches with our numerical observation in Section 5 that the leading order expansion $\tilde{\Psi}_1 \approx \kappa_1(\delta)\zeta$ with $\kappa_1 \rightarrow \infty$ as $\delta \rightarrow 0$.

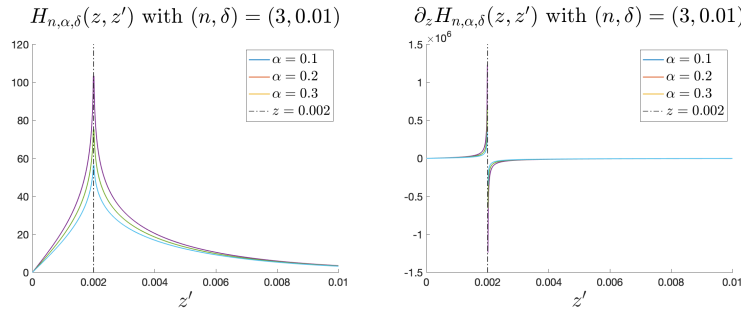


FIG. 20. Profiles of $H_{n,\alpha,\delta}$ and $\partial_z H_{n,\alpha,\delta}$ as functions of z' for different α with $(n, \delta) = (3, 0.01)$ and $z = 0.002$.

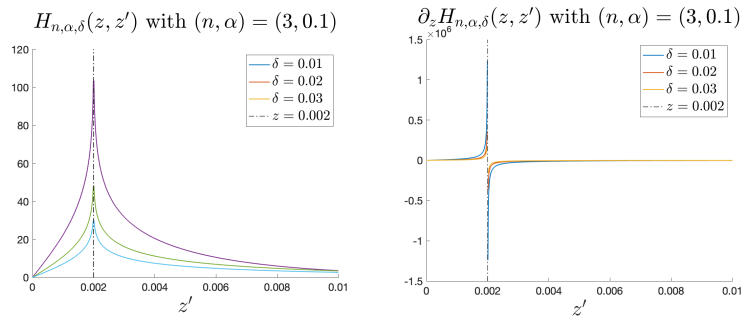


FIG. 21. Profiles of $H_{n,\alpha,\delta}$ and $\partial_z H_{n,\alpha,\delta}$ as functions of z' for different δ with $(n, \alpha) = (3, 0.1)$ and $z = 0.002$.

In Figure 20, 21, and 22, we show the profiles of the kernel functions $H_{n,\alpha,\delta}$ and $\partial_z H_{n,\alpha,\delta}$ for various combinations of (n, α, δ) . Figure 20 shows that the smaller α will make $H_{n,\alpha,\delta}$ and $\partial_z H_{n,\alpha,\delta}$ larger in scale. And this corresponds to the fact that smaller α is easier to develop the blow-up. Figure 21 suggests that the kernel functions

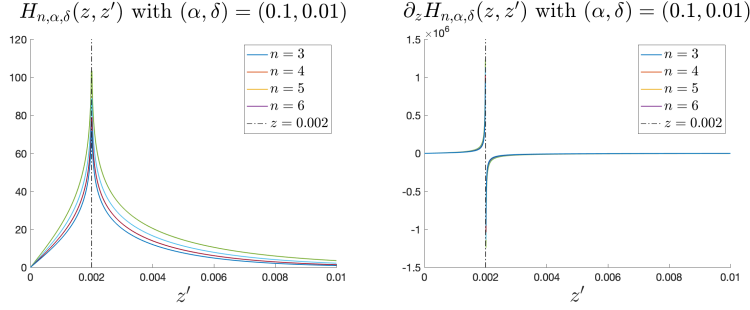


FIG. 22. Profiles of $H_{n,\alpha,\delta}$ and $\partial_z H_{n,\alpha,\delta}$ as functions of z' for different n with $(\alpha, \delta) = (0.1, 0.01)$ and $z = 0.002$.

grow fast as δ approaches zero. Indeed, we can formally expand $H_{n,\alpha,\delta}$ as

$$H_{n,\alpha,\delta} = \frac{1}{\delta} \left(\frac{1}{n+\alpha} A_0 - \frac{n}{2(n+\alpha+2)} A_2 + \frac{n(n+2)}{8(n+\alpha+4)} A_4 + \dots \right),$$

with

$$A_k = \sum_{m \in \mathbb{Z}} \left(\frac{\delta^{n+k}}{(z+m-z')^{n+k}} - \frac{\delta^{n+k}}{(z-m+z')^{n+k}} \right).$$

When z and z' are at the scale of δ and when δ is small, the infinite sum in A_k will be dominated by the term $\frac{\delta^{n+k}}{(z-z')^{n+k}} = \frac{1}{((z-z')/\delta)^{n+k}}$. And this explains why it looks like that the kernel function $H_{n,\alpha,\delta}$ is roughly proportional to $1/\delta$. In Figure 22, we see that as the dimension n increases, the profile of $H_{n,\alpha,\delta}$ seems to become shorter and thinner, which makes the velocity component u^z smaller. This phenomenon is consistent with Table 2 where larger n tends to have slower collapsing speed.

As a possible future study, it is interesting to investigate how the integral transform $T_{n,\alpha,\delta}$ influences the vortex stretching term. If our observation is correct, this 1D model will converge to the original equations as $\delta \rightarrow 0$. But for this 1D model we have a more explicit, though complicated surrogate for the Poisson equation. It would be very interesting to see the interaction between ω_1 and the leading order term in the kernel function $\partial_z H_{n,\alpha,\delta}$ for $\psi_{1,z}$. This will potentially explain the blow-up mechanism in our scenario and may provide crucial insight to our conjectures.

6.2. Numerical Simulation. We note that our assumption of the 1D structure of ω_1 only approximately holds true when δ is very small and the solution is already very close to the steady state. Therefore, we simulate the 1D system numerically using the late stage solution of the equations (2.4) as the initial data. To better resolve the singular profile of ω_1 , we also introduce the dynamic rescaling formulation of (6.1):

$$(6.2a) \quad \tilde{\omega}_{1,\tau} + \left(\tilde{c}_l \zeta + (n-1) \tilde{\psi}_1 \right) \tilde{\omega}_{1,\zeta} = \left(\tilde{c}_\omega - (n-2-\alpha) \tilde{\psi}_{1,\zeta} \right) \tilde{\omega}_1,$$

$$(6.2b) \quad \tilde{\psi}_1 = T'_{n,\alpha,\delta} \tilde{\omega}_1.$$

Here the integral transform for $\tilde{\psi}_1$ is $T'_{n,\alpha,\delta}$. This is to distinguish from $T_{n,\alpha,\delta}$ because they correspond to the different domains (\mathcal{D} and \mathcal{D}') with different boundary conditions.

We consider the settings of $(n, \alpha) = (3, 0.1)$ and $(n, \alpha) = (10, 0.5)$, both with $\delta = 0.001$, as the assumption of our model requires δ to be very small. In Figure 23, we demonstrate the convergence of the scaling factors c_l . We can see that the converged scaling factors c_l in both cases are very close to what we obtained with the original Euler equations. In fact, in both cases the relative difference for c_l is smaller than 2.7×10^{-4} .

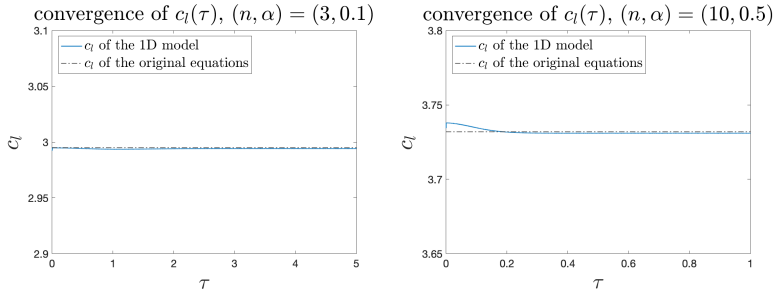


FIG. 23. Convergence of the scaling factors c_l in two cases.

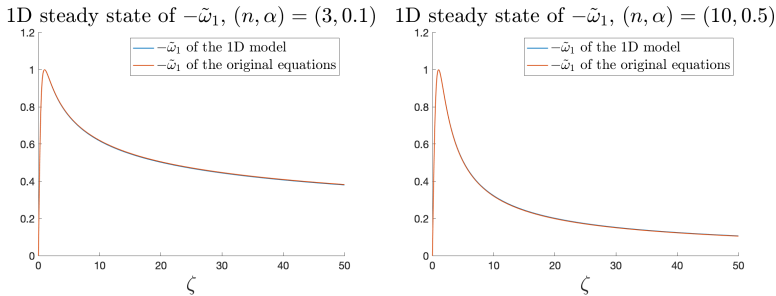


FIG. 24. The comparison of 1D steady states of $-\tilde{\omega}_1$ in two cases.

In Figure 24, we also compare the steady state of the 1D function $\omega_1(z)$ in (6.2) with that obtained by solving the original equations (3.1). We can see that there is no visible difference between the steady states from the 1D model (6.2) and the original equations (3.1). The relative differences in sup-norm for the two cases are at most 4.3×10^{-3} , 2.3×10^{-3} respectively.

7. Concluding remarks. Together with the previous work in [8], we have provided convincing numerical evidence that the n -dimensional axisymmetric Euler equations with no swirl and C^α initial vorticity develops potential finite-time blow-up. The scaling analysis and the dynamic rescaling formulation seem to imply that the potential blow-up is self-similar. This potential blow-up is demonstrated to be computationally robust with respect to the perturbation of initial data, suggesting that the underlying blow-up mechanism is generic and insensitive to the initial data. By introducing a parameter δ to control the stretching of the computational domain and the initial data in the z -axis, we found that the C^α Hölder continuous initial data can develop potential finite-time blow-up when the Hölder exponent α is smaller than some α^* , and this upper bound α^* can asymptotically approach $1 - \frac{2}{n}$ as $\delta \rightarrow 0$. This result supports Conjecture 8 of [5] and generalizes it to the high-dimensional case.

Our numerical observations inspired us to make a few assumptions about the potential blow-up, and to study the limiting case of $\delta \rightarrow 0$. Based on these assumptions, we provide some formal derivation that $\alpha^* = 1 - \frac{2}{n}$ in the limiting case of $\delta \rightarrow 0$, which agrees with our numerical results. For the general case of δ , we noted that the potential self-similar profile tends to have a one-dimensional structure along the z -axis. We further proposed a simple one-dimensional model to capture the leading order behavior of the n -dimensional Euler equations. Our numerical experiments showed that the one-dimensional model is a good approximation of the original equations and can develop approximately the same potential finite-time blow-up as the original n -dimensional Euler equations. We believe that this one-dimensional model captures the leading order behavior of finite-time blow-up of the original n -dimensional Euler equations and can be potentially used to study the finite time blowup of the original Euler equations.

Acknowledgments. The research was in part supported by DMS-2205590. We would like to acknowledge the generous support from Mr. K. C. Choi through the Choi Family Gift Fund and the Choi Family Postdoc Gift Fund.

REFERENCES

- [1] J. CHEN AND T. Y. HOU, *Finite time blowup of 2D Boussinesq and 3D Euler equations with $C^{1,\alpha}$ velocity and boundary*, Communications in Mathematical Physics, 383 (2021), pp. 1559–1667.
- [2] J. CHEN AND T. Y. HOU, *Stable nearly self-similar blowup of the 2D Boussinesq and 3D Euler equations with smooth data*, arXiv preprint arXiv:2210.07191, (2022).
- [3] J. CHEN, T. Y. HOU, AND D. HUANG, *On the finite time blowup of the De Gregorio model for the 3D Euler equations*, Communications on pure and applied mathematics, 74 (2021), pp. 1282–1350.
- [4] M. P. DO CARMO, *Differential geometry of curves and surfaces: revised and updated second edition*, Courier Dover Publications, 2016.
- [5] T. D. DRIVAS AND T. M. ELGINDI, *Singularity formation in the incompressible Euler equation in finite time*, arXiv preprint arXiv:2203.17221, (2022).
- [6] T. M. ELGINDI, *Finite-time singularity formation for $C^{1,\alpha}$ solutions to the incompressible Euler equations on \mathbb{R}^3* , Annals of Mathematics, 194 (2021), pp. 647–727.
- [7] T. Y. HOU, T. JIN, AND P. LIU, *Potential singularity for a family of models of the axisymmetric incompressible flow*, Journal of Nonlinear Science, 28 (2018), pp. 2217–2247.
- [8] T. Y. HOU AND S. ZHANG, *Potential singularity of the axisymmetric Euler equations with C^α initial vorticity for a large range of α . Part I: 3-dimensional case*, arXiv preprint arXiv:2212.xxxxx, (2022).
- [9] M. LANDMAN, G. PAPANICOLAOU, C. SULEM, P. L. SULEM, AND X. P. WANG, *Stability of isotropic self-similar dynamics for scalar-wave collapse*, Physical Review A, 46 (1992), p. 7869.
- [10] M. J. LANDMAN, G. C. PAPANICOLAOU, C. SULEM, AND P.-L. SULEM, *Rate of blowup for solutions of the nonlinear Schrödinger equation at critical dimension*, Physical Review A, 38 (1988), p. 3837.
- [11] B. LEMESURIER, G. PAPANICOLAOU, C. SULEM, AND P. SULEM, *Focusing and multi-focusing solutions of the nonlinear Schrödinger equation*, Physica D: Nonlinear Phenomena, 31 (1988), pp. 78–102.
- [12] J.-G. LIU AND W.-C. WANG, *Convergence analysis of the energy and helicity preserving scheme for axisymmetric flows*, SIAM journal on numerical analysis, 44 (2006), pp. 2456–2480.
- [13] J.-G. LIU AND W.-C. WANG, *Characterization and regularity for axisymmetric solenoidal vector fields with application to Navier–Stokes equation*, SIAM Journal on Mathematical Analysis, 41 (2009), pp. 1825–1850.
- [14] G. LUO AND T. Y. HOU, *Potentially singular solutions of the 3D axisymmetric Euler equations*, Proceedings of the National Academy of Sciences, 111 (2014), pp. 12968–12973.
- [15] G. LUO AND T. Y. HOU, *Toward the finite-time blowup of the 3D axisymmetric Euler equations: a numerical investigation*, Multiscale Modeling & Simulation, 12 (2014), pp. 1722–1776.
- [16] G. LUO AND T. Y. HOU, *Formation of finite-time singularities in the 3D axisymmetric Euler*

- equations: a numerics guided study*, SIAM Review, 61 (2019), pp. 793–835.
- [17] D. W. McLAUGHLIN, G. C. PAPANICOLAOU, C. SULEM, AND P.-L. SULEM, *Focusing singularity of the cubic Schrödinger equation*, Physical Review A, 34 (1986), p. 1200.
 - [18] G. PAPANICOLAOU, C. SULEM, P. L. SULEM, AND X. P. WANG, *The focusing singularity of the davey-stewartson equations for gravity-capillary surface waves*, Physica D: Nonlinear Phenomena, 72 (1994), pp. 61–86.
 - [19] S. ZHANG, *Singularity Formation in the High-Dimensional Euler Equations and Sampling of High-Dimensional Distributions by Deep Generative Networks*, PhD thesis, California Institute of Technology, 2023.